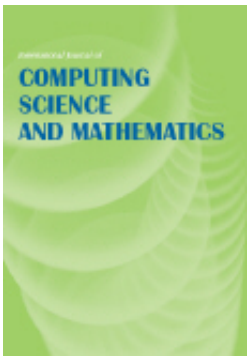

International Journal of Computing Science and Mathematics

ISSN online: 1752-5063 - ISSN print: 1752-5055
https://www.inderscience.com/ijcsm

A synergic deep learning approach for efficient grading of glioma via MRI images

Nirmal Yadav

DOI: 10.1504/IJCSM.2024.10068238

Article History:

Received:	12 April 2024
Last revised:	03 August 2024
Accepted:	19 October 2024
Published online:	06 May 2025

A synergic deep learning approach for efficient grading of glioma via MRI images

Nirmal Yadav

Cluster Innovation Centre,
University of Delhi,
New Delhi, 110007, India
Email: nyadav@cic.du.ac.in
Email: nirmaliitr25@gmail.com

Abstract: Computer-aided diagnosis using deep learning approaches has made tremendous improvements in medical imaging for automatically detecting tumor area, tumor type, and grading of the tumor. These advancements are limited due to the fact that (1) medical images are often less in quantity, leading to overfitting, and (2) significant inter-class similarity and intra-class variation between the images. The main aim of the study is to develop a deep learning base model (Zhang et al., 2018; 2019; Krizhevsky et al., 2012) as a backbone for the automatic grading of glioma tumors. The synergic deep learning (SDL) architecture enables two pre-trained models to learn from each other mutually and allows them to perform better than vanilla pre-trained models. Our study uses T1-weighted sagittal tumor magnetic resonance imaging (MRI) slices from the REMBRANDT (Scarpace et al., 2019) dataset. The proposed architecture achieves an accuracy of 98.36%, showing that the model achieves excellent performance metrics on a small dataset.

Keywords: glioma tumour grading; SDL; synergic deep learning; transfer learning; AlexNet; REMBRANDT.

Reference to this paper should be made as follows: Yadav, N. (2025) 'A synergic deep learning approach for efficient grading of glioma via MRI images', *Int. J. Computing Science and Mathematics*, Vol. 21, No. 1, pp.1–13.

Biographical notes: Nirmal Yadav, PhD, is currently working as an Assistant Professor at Cluster Innovation Center, University of Delhi, India. Her area of research is medical imaging.

1 Introduction

Glioma is the second most prevalent brain tumour in adults after meningiomas. The earliest documented accounts of gliomas were published by Berns in British scientific journals in 1800. Percival Bailey and Harvey Cushing established the foundation for the contemporary classification of gliomas in 1926. As per a National Library of Medicine journal, there are six cases of gliomas diagnosed annually per 100,000 individuals in US Mesfin and Al-Dhahir (2021). Gliomas are tumours that infiltrate the surrounding brain tissue diffusely. They are classified by the World Health Organization's malignancy

scale into grades I to IV. Pilocytic astrocytoma, the most common glioma in children, is a benign grade I lesion that has a slow proliferation rate and is relatively well-defined. Grade II tumours, such as astrocytoma, oligodendroglioma, and oligoastrocytoma, have a slow growth rate, are highly differentiated, and infiltrate the normal brain parenchyma diffusely, making them prone to malignant progression. Anaplastic astrocytoma, anaplastic oligodendroglioma, and anaplastic oligoastrocytoma are grade III tumours that exhibit higher cellular density and have atypia and mitotic cells. Glioblastoma and gliosarcoma are the most malignant grade IV tumours and are also the most common gliomas. They exhibit microvascular proliferation and pseudo-palisading necrosis in addition to grade III features. For gliomas, MRI is particularly valuable, and conventional MRI protocols using T1-weighted, T2-weighted, and gadolinium-enhanced sequences play a significant clinical role. These protocols provide high-resolution structural information in multiple planes, enabling better tissue characterisation compared to CT (Upadhyay and Waldman, 2011). In the field of diagnostic imaging, there has been a significant increase in the number of publications on AI, from approximately 100–150 per year in 2007–2008 to 1000–1100 per year in 2017-2018 (Tang, 2020). Some studies used by Researchers have utilised AI to automatically identify complex patterns in imaging data and provide quantitative assessments of radiographic features (Singh and Yadav, 2014).

Imaging is crucial for the diagnosis, surveillance, characterisation, and therapeutic monitoring of intracranial tumours. The limited quantity of datasets in medical image analysis, along with the significant intra-class variation and inter-class similarity, present an even greater challenge in classifying medical images. The synergic deep learning (SDL) model allows for the simultaneous learning of multiple image pairs and utilises multiple deep convolution neural network (DCNN) components without sharing parameters, enabling the model to benefit from an ensemble of multiple networks. This model can be trained end-to-end using classification errors from DCNNs and synergic errors from each pair of DCNNs. If one DCNN correctly classifies an image, the synergic error generated by the other DCNN serves as an additional force to update the model. The Synergic Deep Learning model was first proposed for the task of Skin Lesion Classification in Dermoscopy Images. SDL model used ResNet50 as its backbone and achieved an accuracy of 85.75%, average precision of 66.4%, and area under the curve (AUC) of 82.6% on the International Skin Imaging Collaboration (ISIC) 2016 (Gutman et al., 2016) skin classification dataset. The accuracy achieved by the model was greater than the accuracy of ResNet50, ResNet502, and the other top 5 performing models on the leaderboard. That proposed model performed better than a joint segmentation-classification model. A generalised SDLn model was study on different datasets i.e., ImageCLEF-2015 (García Seco de Herrera et al., 2015), ImageCLEF-2016 (García Seco de Herrera et al., 2016), ISIC-2016, and ISIC-2017 (Codella et al., 2018). The results of SDLn are outperformed by the existing state-of-the-art models, including ResNet50 and ResNet502. However, the study emphasised the need for synthetic deep Learning Models for medical image classification and analysis. Thus SDL model has been employed for several diverse datasets, including a study on Diabetic Retinopathy (Kathiresan et al., 2020). The paper focused on the classification of DR fundus images and achieved an accuracy of 99.28%, a sensitivity of 98%, and a specificity of 99%.

A recent research on the Grading of glioma tumours using Deep Learning (Gutta et al., 2021) trained a joint segmentation-classification pipeline using Convolutional Neural Networks and achieved an average accuracy of 87% on a dataset of 237 patients. Their model outperformed the methods considering radiomic features alone and also shows the highest performing model (gradient boosting). Xiao et al. (2019) involved integrating

radiomics features with high-level deep learning features to construct a more comprehensive representation of medical images. The features were extracted using a fine-tuned VGG-16 model, and the BRATS 2018 (Bakas et al., 2017(a,b) dataset was used, which includes 285 subjects from multiple institutions. The extracted features were then utilised to train three classifiers, namely Logistic Regression (LR), support vector machine (SVM), and linear discriminant analysis (LDA). Moreover, the best results were achieved by combining radionics feature extraction with deep learning feature extraction. The recursive feature elimination (RFE) algorithm was used for feature selection. This method achieved an average accuracy of 89.1% and an average AUC of 93.4%. Another study (Babu and Sourirajan, 2017) used the Rembrandt dataset for the detection of brain tumours, specifically for tumour grading. To recognise tumours from brain MRI images, the Tetrolet Transform (TT) (Krommweh, 2010) and SVM classifier were employed (Latif et al., 2022). The Tetrolet transform was used to decompose the MRI brain tumour image at a predefined level, and the resulting image features were then classified using SVM. The fifth level of decomposition with SVM-based classification resulted in an accuracy level of 98.8%. In addition, machine learning-based models have provided good performance architectures for the classification and segmentation of the brain tumour (Nalepa et al., 2023; Habib et al., 2021; Sajjad et al., 2019; Díaz-Pernas et al., 2021).

In this work, a SDL model with an AlexNet backbone for classifying the grade of a glioma tumour to MRI slices has been proposed. The SDL-based architecture for grading glioma tumours provides high accuracy even with a small training dataset. This efficiently facilitates the training process and also reduces the problem of insufficient data for training the modal. The pre-trained AlexNet models aim to prevent overfitting caused due to the low number of MRI slices and the overall SDL architecture allows two AlexNets to mutually learn from each other. Each DCNN is trained separately, and then the extracted feature vector for an image is fed into the synergic layer, which predicts if the two images passed through two DCNNs belong to the same class. The error produced in the synergic layer is back propagated to the DCNNs, allowing them to learn from each other. The most promising advantage of using this approach is that it eliminates the necessity of a large dataset for the prediction and grading of glioma. When compared with other deep learning-based approaches, SDL architecture recognises the critical information from the training pictures and thus exhibits better accuracy in the classification process. Also, in this process, the most promising image classification structure, i.e., AlexNet, is used to provide extensive results to detect abnormalities in medical imaging.

Moreover, this paper makes the following contributions:

- A SDL model with an AlexNet backbone fine-tuned on an extremely small subset of the REMBRANDT dataset (T1-weighted sagittal - assorted scanning views).
- Deep Learning-based model has been developed with an accuracy of 98.36%, an average precision of 89.80%, an average recall of 92.3%, and an average F1 score of 90.91%.
- Comparison with models in the literature with results showing that the proposed model either outperforms or performs equally, even after being trained on a smaller dataset.
- A first-of-its-kind open-source implementation of the SDL model.
- Discussions on the REMBRANDT dataset, stability interval of the synergic hyper-parameter, the use of Gaussian filters, and AlexNet as a backbone for SDL.

2 Proposed architecture

The architecture of the proposed work includes preprocessing of the dataset and a SDL model. A detailed description of these steps is given below.

2.1 Pre-processing

The T1-weighted sagittal MRI slices were selected as the tumour was visible in these scans. Figure 1 shows some sample images from the dataset that have been used while training the classification model. This was done to address the fact that a large number of axial images contained no information about the tumour, but we could see the tumour in almost all the sagittal images.

Figure 1 First 2 images (both grade 3 tumour) depicting intra-class variation and last 2 images (from left to right: grade 4 and grade 3) depicting inter-class similarity

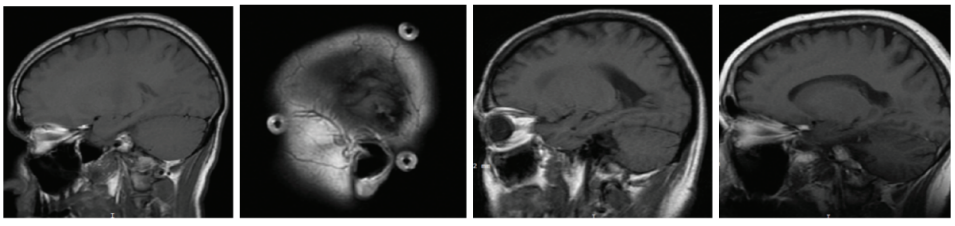

The images were augmented to increase the size of the dataset. The augmentation process included randomly rotating the images in the range of $\pm$ 10 degrees and applying Gaussian filters of kernel sizes 3×3, 5×5, and 7×7.

2.2 Synergic deep learning model

The SDL model is used to extract a useful set of feature vectors from the segmented images. The SDL model consists of three main modules: an input layer with 3 labels, 2 independent DCNNs, and a synergic layer. The first layer takes paired images as input, which are selected from the dataset. Figure 2 shows a diagrammatic description of the SDL model. The synergic label conveys that if a pair of images belong to the same class, then it shows (1); otherwise, (0). Images belonging to each grade were randomly shuffled, and the first 50% of images belonging to a particular grade were paired with each other, giving them a synergic label of 1. The remaining 50% of the images were paired randomly with an image of another grade, giving them a synergic label of 0. This split also resulted in a loss of images; the last set of images could not be paired up with an image belonging to a different grade, as all the remaining images had the same grading. The input layer is then passed the information to the two DCNN components. DCNN components understand image representation independently with the help of class labels. During forward propagation, the feature vector of the pair of images is obtained from the second last layer of each DCNN and is concatenated for the synergic layer. This concatenated feature vector is fed to the synergic layer, which then predicts if the images belong to the same class or not.

Figure 2 Diagrammatic representation of the proposed synergic deep learning model (see online version for colours)

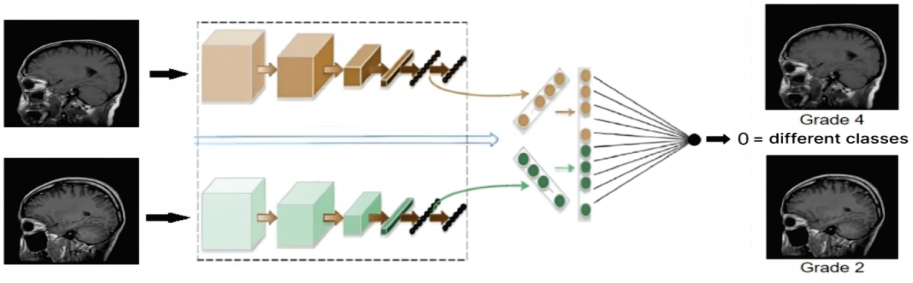

Figure 3 Architecture of our data pipeline and model

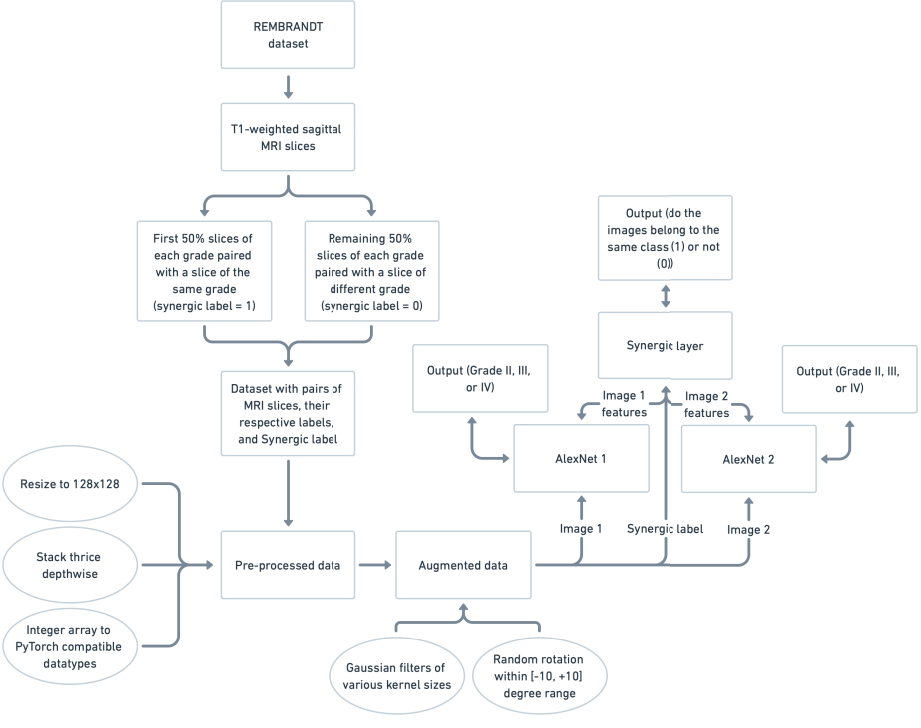

For a data pair Z_A,Z_B with labels y_A,y_B where $A \neq B$, the synergic label y_s is defined as:

$$y_s = \begin{cases} 1 & y_A = y_B \\ 0 & y_A \neq y_B \end{cases} \tag{1}$$

Given that the MRI slices have only 1 channel and the pre-trained models accept images with 3 channels, every image was stacked depthwise to make the resulting image have 3 channels where each channel held the same information. After pairing images, the dataset was split in a ratio of 7:3 for the training and testing phase. and every MRI slice was resized to 128×128 to allow the model to converge faster. In this work, we use 2 AlexNets as the

DCNN components, with their classification layer replaced by a single layer of neurons followed by the prediction layer of 3 neurons. We also define a single neuron layer as the synergic layer with 1 output neuron and sigmoid activation to predict the synergic label. The synergic layer of the SDL model minimises the following binary cross-entropy loss:

$$Loss_{SDL} = y_s \log \hat{y_s} + (1 - y_s) \log (1 - \hat{y_s}) \tag{2}$$

and the DCNN components are trained to minimise the following Cross Entropy (CE):

$$Loss_{DCNN} = \sum_{i=1}^{n} \sum_{c=1}^{3} y_{ic} \log p_{ic} \tag{3}$$

where n is the batch size, c is the number of classes, and p is the predicted probability of the DCNN component. Figure 3 shows the architecture of the model's data pipeline and the double-headed arrows in the model section depicting both the forward and the back propagation process as given in Zhang et al. (2019).

3 Experiments

3.1 Dataset

The REMBRANDT dataset used in this study was obtained through The Cancer Imaging Archive (TCIA) Clark et al. (2013). The dataset houses MRI slices of 127 patients stored in the DICOM format and the typical folder structure used for storing DCM MRI slices. It contains image scans of 89 patients of distinct ages, races, and maladies and contains glioma grading information. From this dataset, we selected all the T1-weighted sagittal MRI slices. The selected 417 slices are described in Table 1. These selected images are divided into two sets for training and testing purposes. The training set consists of 295 slices, and the testing set with 122 slices.

Table 1 Selected dataset description

Grade	*Patients*	*Selected Slices*
II	41	128
III	25	108
IV	23	181

3.2 Evaluation metrics

For comparison with the previous models, the experiment performance can be illustrated by using the following metrics

$$Precision = \frac{True\ positive}{True\ positive + False\ positive} \tag{4}$$

$$Sensitivity = \frac{True\ positive}{True\ positive + False\ negative} \tag{5}$$

$$Specificity = \frac{True\ negative}{True\ positive + False\ positive} \tag{6}$$

$$Accuracy = \frac{True\ positive + True\ negative}{True\ positive + False\ positive + True\ negative + False\ negative} \tag{7}$$

3.3 Results

In this section, the experimental results for the proposed methodology have been illustrated. The training and testing were performed on a machine with 8GB RAM, Intel-i5-10300H CPU @ 2.5 GHz, and a dedicated NVIDIA GTX 1650ti GPU. Training of the model took 1281 s for 184 pairs of images, making each epoch last for an average of 5.124 s. The training is performed on 70% of the total dataset, and the remaining dataset is used for testing. n this experiment, the model was trained for 250 epochs with the data divided into a batch size of 8, and it was trained using a Stochastic Gradient Descent optimizer with an initial learning rate of 0.0001. The model achieved the highest accuracy of 98.36% with the synergic hyper-parameter λ set to 3. For different values of the synergic hyperparameter, λ within the stability interval as described in Zhang et al. (2019), it is being noted that the accuracy of the SDL model went down as we increased the value of λ. Figure 4(a) shows the accuracy graph for both the DCNNs from the SDL model with $\lambda = 3$, and it indicates that the accuracies of both the DCNNs converge. Figure 4(b) shows the loss values for the same DCNNs, and it can be observed that both the loss functions converge as well. Furthermore, Figure 5 shows the loss and accuracy of the synergic layer, the layer that was responsible for classifying the pair of images passed to the DCNNs as 1 (same class) or 0 (different class). It can be observed that the synergic layer quickly attains an accuracy of 100%, and the loss function first fluctuates but soon converges exactly to 0.

The experimental outcomes of the proposed framework are studied for different number of epochs. The testing accuracies and losses of the DCNN components of the SDL model fluctuate but converge at the same time, as shown in Figure 4(a) and (b). The DCNN components from the best SDL model achieved an accuracy of 98.36%. The experiment was performed on 250 epochs, and the results show that the best accuracy was not achieved in the last epoch; rather, it was achieved in an intermediate epoch. Further, the value of the synergic hyper-parameter λ was varied from 3 to 8 and recorded the highest testing and training accuracies achieved by the proposed model. It was observed that as λ increases, the training accuracy varies only by a small factor, whereas the variation in the testing accuracy is noticeable. More specifically, as the kernel size of the Gaussian filter increased, the accuracy went down, as shown in Figure 6. Finally, Figure 7 depicts the images for the classification results obtained from the input MRI image dataset to the proposed classification model. This is divided into two horizontal halves, with the upper half containing a vertical pair of images with synergic label 1 and the lower half containing a vertical pair of images with synergic label 0. Each image includes the original label of the slice and the label predicted by the two DCNNs.

Table 2 compares the SDL model with other pre-trained models and models available in the literature. The implemented model was found satisfactory in almost all the measures used for comparison with other state-of-the-art models. Table 3 shows the outcomes of various performance metrics obtained for all three grades after the classification, and it can be observed that the model performed constantly in terms of accuracy and other metrics.

Figure 4 Accuracy and loss curves of the proposed model: (a) accuracy vs epochs for two DCNNs and (b) loss vs epoch for two DCNNs (see online version for colours)

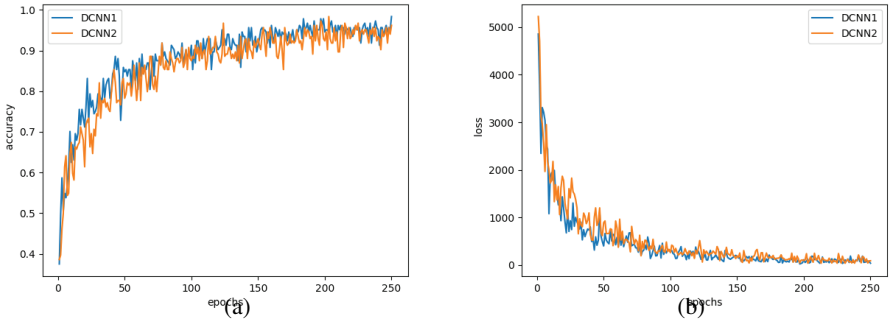

(a) (b)

Figure 5 Model accuracy and loss during a synergic phase (see online version for colours)

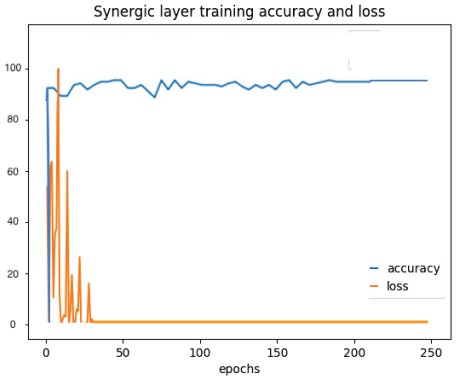

Figure 6 Varying synergic parameter and Gaussian filter size: (a) accuracy vs. lambda for the proposed model and (b) accuracy vs. Gaussian filter size for proposed model (see online version for colours)

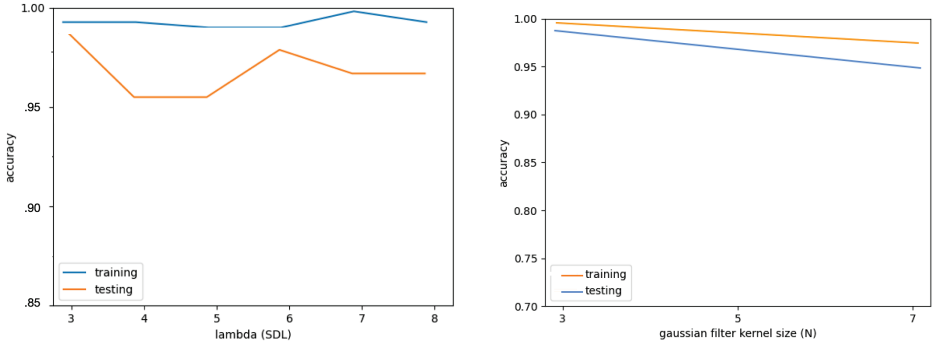

(a) (b)

Figure 7 The upper horizontal half contains three vertical pairs of images with synergic label 1, and the lower half contains three vertical pairs of images with synergic label 0. Each image includes the original label of the slice and the label predicted by the two DCNNs.* L = Label, P = prediction

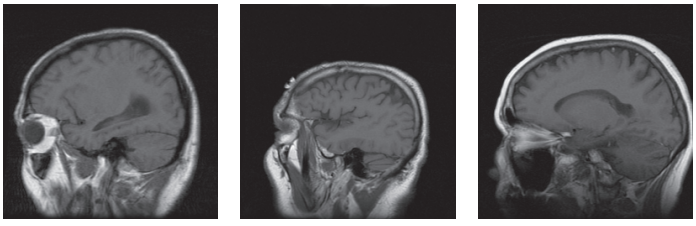

(a1) L = 4, P= (4, 2). (b1) L= 2, P= (2, 2). (c1) L= 3, P= (3, 3).

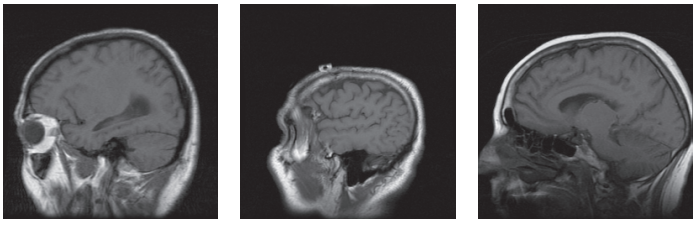

(a2) L = 4, P= (4, 4). (b2) L = 2, P= (2, 2). (c2) L= 3, P= (3, 3).

(a) Synergic label = 1 (b) Synergic label = 1 (c) Synergic label = 1

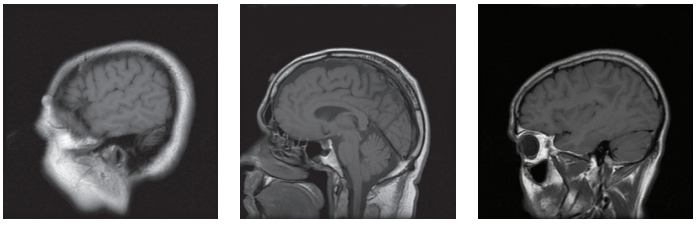

(d1) L= 2, P= (2, 4). (e1) L= 2, P= (2, 2). (f1) L= 3, P= (3, 3).

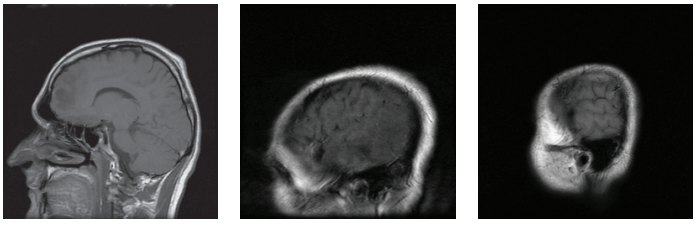

(d2) L= 3, P= (3, 3). (e2) L= 4, P= (4, 4). (f2) L= 4, P= (2, 4).

(d) Synergic label = 0 (e) Synergic label = 0 (f) Synergic label = 0

In this study, AlexNet was chosen over the ResNet models for the backbone of the model to avoid overfitting. The ResNet models are comparatively bigger and have a more complicated

architecture than the AlexNet model, which led to the SDL model having a high variance while training and other smaller models like VGG19 led to the SDL model having a high bias; hence, the AlexNet model a best suitable option for the backbone of SDL. An independently fine-tuned AlexNet performed poorly on the testing dataset with an accuracy of 78.57%, average precision of 77.15%, average recall of 74.44%, and average F1 score of 75.10%. However, the same pre-trained model, when fine-tuned within the SDL architecture, performs exceptionally well and gives good results on both the training and testing data.

Table 2 Comparing the proposed SDL model with popular pre-trained models

Model	*Accuracy*	*Precision*	*Specificity*	*Sensitivity*
Proposed model	98.36	**96.05**	**97.19**	**96.07**
CNN model (Irmak, 2021)	**98.14**	85.19	92.66	81.11
Sajjad (Sajjad et al., 2019)	**90.67**	81.84	80.88	78.89
Kabir (Kabir et al., 2019)	**90.90**	**92.92**	87.04	87.04
Naser 2020 (Naser and Deen, 2020)	**89.00**	N/A	92.02	87.19

Table 3 Classwise classification report

Grade	*Accuracy*	*Precision*	*Sensitivity*	*Specificity*
II	96.6	98.0	95.8	98.1
III	**100**	98.89	**100**	**97.06**
IV	97.30	**95.38**	97.30	97.74

4 Conclusion

This paper presented a SDL model with an AlexNet backbone for automated grading (II, III, and IV) of glioma tumour MRI scans to overcome the 2 prevalent problems present in medical image classification models - 1. Overfitting, and 2. Significant intra-class variation and inter-class similarity. This study used a small subset of the REMBRANDT dataset, for the training of the model and demonstrated equal proficiency when compared to several other models trained on comparatively larger datasets. Adding a Gaussian filter to the SDL model brought down both the training and the testing accuracies. Additionally, increasing the kernel size of the Gaussian filter further brought down the accuracy of the SDL model. Further, the best SDL model (at $\lambda = 3$) gave us an average precision of 96.05%, 97.19% specificity, and 96.07% sensitivity.

Funding

This research received no external funding.

Conflicts of interest

The authors declare that they have no known competing financial interests or personal relationships that could have appeared to influence the work reported in this paper.

References

Babu, B. and Sourirajan, V. (2017), 'Detection of brain tumour in MRI scan images using tetrolet transform and SVM classifier', *Indian Journal of Science and Technology*, Vol. 10, pp.1–10.

Bakas, S., Akbari, H., Sotiras, A., Bilello, M., Rozycki, M., Kirby, J., Freymann, J., Farahani, K. and Davatzikos, C. (2017(a)) 'Advancing the cancer genome atlas glioma mri collections with expert segmentation labels and radiomic features', *Scientific Data*, Vol. 4, p.170117, https://doi.org/10.1038/sdata.2017.117

Bakas, S., Akbari, H., Sotiras, A., Bilello, M., Rozycki, M., Kirby, J., Freymann, J., Farahani, K. and Davatzikos, C. (2017b) *Segmentation Labels for the Pre-operative Scans of the TCGA-GBM Collection [Data set]*, The Cancer Imaging Archive, DOI: 10.7937/K9/TCIA.2017.KLXWJJ1Q

Clark, K., Vendt, B., Smith, K., Freymann, J., Kirby, J., Koppel, P., Moore, S., Phillips, S., Maffitt, D., Pringle, M., Tarbox, L. and Prior, F. (2013) 'The cancer imaging archive (TCIA): Maintaining and operating a public information repository', *Journal of Digital Imaging*, Vol. 26, pp.1045–1057.

Codella, N.C.F., Gutman, D., Celebi, M.E., Helba, B., Marchetti, M.A., Dusza, S.W., Kalloo, A., Liopyris, K., Mishra, N., Kittler, H. and Halpern, A. (2018) 'Skin lesion analysis toward melanoma detection: a challenge at the 2017 International symposium on biomedical imaging (ISBI), hosted by the international skin imaging collaboration (ISIC)', *2018 IEEE 15th International Symposium on Biomedical Imaging (ISBI 2018)*, Washington, DC, USA, pp.168–172, doi: 10.1109/ISBI.2018.8363547.

Díaz-Pernas, F.J., Martínez-Zarzuela, M., Antón-Rodríguez, M. and González-Ortega, D. (2021) 'A deep learning approach for brain tumor classification and segmentation using a multiscale convolutional neural network', *Healthcare*, Vol. 9, No. 2, https://doi.org/10.3390/healthcare9020153

García Seco de Herrera, A., Müller, H. and Bromuri, S. (2015) P*Overview of the ImageCLEF 2015 Medical Classification Task*, Working Notes of CLEF 2015 (Cross Language Evaluation Forum).

García Seco de Herrera, A., Schaer, R., Bromuri, S. and Müller, H. (2016) *Overview of the ImageCLEF 2016 Medical Task*, Working Notes of CLEF 2016 (Cross Language Evaluation Forum).

Gutman, D., Codella, N.C.F., Celebi, E., Helba, B., Marchetti, M., Mishra, N. and Halpern, A. (2016) 'Skin lesion analysis toward melanoma detection', *A Challenge at the International Symposium on Biomedical Imaging (ISBI)*, International Skin Imaging Collaboration (ISIC), DOIarXiv:1605.01397.

Gutta, S., Acharya, J., Shiroishi, M., Hwang, D. and Nayak, K. (2021) 'Improved glioma grading using deep convolutional neural networks', *American Journal of Neuroradiology*, Vol. 42, No. 2, pp.233–239.

Habib, H., Amin, R., Ahmed, B. and Hannan, A. (2021) 'Hybrid algorithms for brain tumor segmentation, classification, and feature extraction', *Journal of Ambient Intelligence and Humanized Computing*, No. 5, pp.2763–2784, DOI https://doi.org/10.1007/s12652-021-03544-8

Irmak, E. (2021) 'Multi-classification of brain tumor mri images using deep convolutional neural network with fully optimized framework', *Iranian Journal of Science and Technology*, Vol. 45, pp.1015–1036.

Kabir, A.A., Ayati, M. and Kazemi, F. (2019) 'Magnetic resonance imaging-based brain tumor grades classification and grading via convolutional neural networks and genetic algorithms', *Biocybern Biomedical Engineering*, Vol.39, No. 1, pp.63–74.

Kathiresan, S., Sait, A. R.W., Gupta, D., S.K,L., Khanna, A. and Pandey, H.M. (2020) 'Automated detection and classification of fundus diabetic retinopathy images using synergic deep learning model', *Pattern Recognition Letters (Elsevier)*, Vol. 133, pp.210–216.

Krizhevsky, A., Sutskever, I. and Hinton, G.E. (2012) 'ImageNet classification with deep convolutional neural networks', *Communications of the ACM*, Vol. 60, pp.84–90.

Krommweh, J. (2010) 'Tetrolet transform: A new adaptive HAAR wavelet algorithm for sparse image representation', *Journal of Visual Communication and Image Representation*, Vol. 21, pp.364–374.

Latif, G., Ben Brahim, G, Iskandar, D.N.F.A., Bashar, A. and Alghazo, J. (2022) 'Glioma tumors' classification using deep-neural-network-based features with SVM classifier', *Diagnostics (Basel)*, Vol. 12, No. 4, 18 April, p.1018, doi: 10.3390/diagnostics12041018.

Mesfin, F. and Al-Dhahir, M. (2021) '*Gliomas*, StatPearls, StatPearls Publishing, TreasureIsland, FL.

Nalepa, J., Kotowski, K., Machura, B., Adamski, S., Bozek, O., Eksner, B., Kokoszka, B., Pekala, T., Radom, M., Strzelczak, M., Zarudzki, L., Krason, A., Arcadu, F. and Tessier, J. (2023) 'Deep learning automates bidimensional and volumetric tumor burden measurement from MRI in pre- and post-operative glioblastoma patients', *Computers in Biology and Medicine*, Vol. 154, pp.1–19.

Naser, M.A. and Deen, M.J. (2020) 'Brain tumor segmentation and grading of lower-grade gliomausing deep learning in MRI images', *Computers in Biology and Medicine*, Vol. 121, Doi https://doi.org/10.1016/j.compbiomed.2020.103758

Sajjad, M., Khan, S., Muhammad, K., Wu, W., Ullah, A. and Baik, S.W. (2019) 'Multi-grade brain tumor classification using deep CNN with extensive data augmentation', *Journal of Computational Science*, Vol. 30, pp.174–182.

Scarpace, L., Flanders, A.E., Jain, R., Mikkelsen, T. and Andrews, D.W. (2019) 'Data from REMBRANDT [data set]', *The Cancer Imaging Archive*, DOI: 10.7937/K9/TCIA.2015.588OZUZB.

Singh, C., Yadav, D. and Lee, J. (2014) 'Reader comprehension ranking by monitoring eye gaze using eye tracker', *International Journal of Intelligent Systems Technologies and Applications*, Vol. 13, No. 4, pp.294–307, https://doi.org/10.1504/IJISTA.2014.068831

Tang, X. (2020) 'The role of artificial intelligence in medical imaging research', *BJR|Open*, Vol. 2, No. 1, pp.20190031.

Upadhyay, N. and Waldman, A. (2011) 'Conventional MRI evaluation of gliomas', *The British Journal of Radiology*, Vol. 84 Spec No. 2, pp.S107–S11.

Xiao, T., Hua, W., Li, C. and Wang, S. (2019) 'Glioma grading prediction by exploring radiomics and deep learning features', *Proceedings of the Third International Symposium on Image Computing and Digital Medicine, ISICDM 2019*, Association for Computing Machinery, New York, NY, USA, pp.208–213.

Zhang, J., Xie, Y., Wu, Q. and Xia, Y. (2018) 'Skin lesion classification in dermoscopy images using synergic deep learning', in Frangi, A.F., Schnabel, J.A., Davatzikos, C., Alberola-López, C. and Fichtinger, G. (Eds.): *Medical Image Computing and Computer Assisted Intervention – MICCAI 2018*, Springer International Publishing, Cham, pp.12–20.

Zhang, J., Xie, Y., Wu, Q. and Xia, Y. (2019) 'Medical image classification using synergic deep learning', *Medical Image Analysis*, Vol. 54, pp.10–19.